

FIXED-NODE DMC FOR FERMIONS ON A LATTICE: APPLICATION TO THE DOPED FULLERIDES

ERIK KOCH AND OLLE GUNNARSSON

*Max-Planck-Institut für Festkörperforschung
Heisenbergstraße 1, 70569 Stuttgart, GERMANY*

AND

RICHARD M. MARTIN

*Department of Physics and Materials Research Laboratory
University of Illinois, 1110 W. Green Street, Urbana, IL, USA*

1. Introduction

Why should we use lattice Monte Carlo methods to describe a real system when there are so many efficient and accurate methods to treat the full problem? There are at least two good reasons. The first one takes a pragmatic point of view: For complicated systems a full calculation simply cannot be done on present-day computers. The second reason rests on the belief that the physics underlying the properties of real materials is simple and can be captured in model systems. If we succeed in this there is the additional benefit of having identified the important general features of the material.

For the doped Fullerides we encounter just such a situation. Even for a single C_{60} molecule a full QMC calculation is still a challenge, and simulations of Fullerides, i.e. solids made of C_{60} molecules, are simply out of question. For many properties it is, however, sufficient to focus on the valence band only, removing all other degrees of freedom from the Hamiltonian. Important features of the doped Fullerides that have to be reflected in such a model are the degeneracy of the molecular orbital that gives rise to the valence band, the filling of the valence band, and the lattice structure of the solid. All these can be incorporated in a Hubbard-like Hamiltonian, which can be treated efficiently using lattice QMC methods.

In the following we will first show how to set up a model Hamiltonian for the doped Fullerides. Then we discuss Monte Carlo methods for such lat-

tice Hamiltonians, especially the optimization of Gutzwiller functions both in variational and fixed-node diffusion Monte Carlo. Finally we use QMC to investigate the Mott transition in the doped Fullerenes. The interest in these questions comes from the following situation: Density functional calculations predict that the doped Fullerenes are metals. On the other hand, one finds that the Coulomb repulsion between electrons on the same C_{60} molecule is very strong. This suggests that correlations should be dominating, making all doped Fullerenes Mott insulators. Reality falls in between these two extremes: some doped Fullerenes are metals (and even superconductors), while others are insulators. From our QMC calculations we find that due to the degeneracy of the valence band the integer-doped Fullerenes are close to a Mott transition, and not far into the Mott insulator regime, as simple theories would suggest. Whether a given compound is on the metallic or the insulating side of the transition depends then on the crystal structure (bipartite vs. frustrated) and the filling of the band.

2. Model Hamiltonian

Solid C_{60} is characterized by a very weak inter-molecular interaction. Therefore the discrete molecular levels merely broaden into narrow, well separated bands (see Fig. 1) [1]. The valence band originates from the lowest unoccupied molecular orbital, which is a 3-fold degenerate t_{1u} orbital. Doping the solid with alkali metals does not affect the band structure close to the Fermi level very much. Only the filling of the t_{1u} band changes, since each alkali atom donates its valence electron. To simplify the description of the doped Fullerenes we want to focus on the electrons in the t_{1u} band only. To get rid of the other degrees of freedom we use the Löwdin downfolding technique [2]. The basic idea is to partition the Hilbert space into a subspace that contains the degrees of freedom that we are interested in (in our case the ‘ t_{1u} -subspace’) and the rest of the Hilbert space: $\mathcal{H} = \mathcal{H}_0 \oplus \mathcal{H}_1$. We can then write the Hamiltonian of the system as

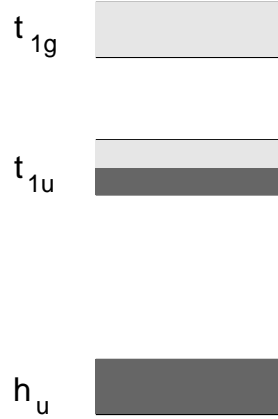


Figure 1. : Schematic band structure of A_3C_{60} .

$$H = \begin{pmatrix} H_{00} & 0 \\ 0 & H_{11} \end{pmatrix} + \begin{pmatrix} 0 & V_{01} \\ V_{10} & 0 \end{pmatrix}, \quad (1)$$

where H_{ii} is the projection of the Hamiltonian onto subspace \mathcal{H}_i , while $V_{ij} = H_{ij}$ contain the hybridization matrix elements between the two subspaces. Writing Green’s function $G = (E - H)^{-1}$ in the same way, we can

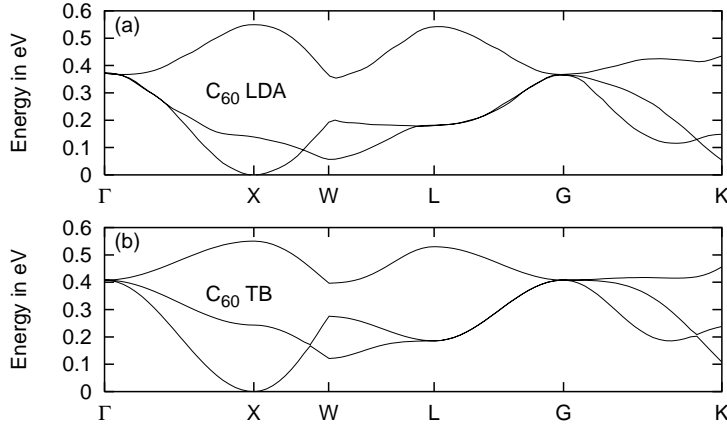


Figure 2. Band structure (t_{1u} band) of solid C_{60} (fcc) (a) as calculated *ab initio* using the local density approximation [1] and (b) using a tight-binding Hamiltonian with only t_{1u} orbitals [4].

calculate the projection of G onto \mathcal{H}_0 [3]:

$$G_{00} = \left(E - \underbrace{[H_{00} + V_{01}(E - H_{11})^{-1}V_{10}]}_{H_{\text{eff}}(E)} \right)^{-1}. \quad (2)$$

We see that the physics of the full system is described by an effective Hamiltonian $H_{\text{eff}}(E)$ that operates on the subspace \mathcal{H}_0 only. This drastic simplification comes, however, at a price: the effective Hamiltonian is energy dependent. In practice one approximates it with an energy-independent Hamiltonian $H_{\text{eff}}(E_0)$. This works well if we are only interested in energies close to E_0 . In solid C_{60} we have the fortunate situation that the bands retain the character of the molecular orbitals, since the hybridization matrix elements are small compared to the energy separations of the orbitals. In fact we can neglect the other bands altogether and get the hopping matrix elements $t_{in,jn'}$ between the t_{1u} orbitals n and n' on molecules i and j directly from a tight-binding parameterization [4, 5]. Figure 2 shows the comparison of the *ab initio* t_{1u} band structure with the band structure obtained from the tight-binding Hamiltonian with only t_{1u} orbitals.

To get a realistic description of the electrons in the t_{1u} band we have to include the correlation effects which come from the Coulomb repulsion of electrons in t_{1u} orbitals on the same molecule. The resulting Hamiltonian which describes the interplay of the hopping of electrons and their Coulomb repulsion has the form

$$H = \sum_{\langle ij \rangle} \sum_{nn'\sigma} t_{in,jn'} c_{in\sigma}^\dagger c_{jn'\sigma} + U \sum_i \sum_{(n\sigma) < (n'\sigma')} n_{in\sigma} n_{in'\sigma'}. \quad (3)$$

The on-site Coulomb interaction U can be calculated within density functional theory [6]. It is given by the increase in the energy of the t_{1u} level per electron that is added to one molecule of the system. It is important to avoid double counting in the calculation of U . While the relaxation of the occupied orbitals and the polarization of neighboring molecules has to be included in the calculation, excitations within the t_{1u} band must be excluded, since they are contained explicitly in the Hamiltonian (3). The results are consistent with experimental estimates [7, 8]: $U \approx 1.2 - 1.4 \text{ eV}$. For comparison, the width of the t_{1u} band is in the range $W \approx 0.5 - 0.85 \text{ eV}$.

3. Quantum Monte Carlo

We now turn to the question of how to calculate the ground state of a lattice Hamiltonian like (3). To simplify the notation most examples in the present section are for the simple Hubbard model (only one orbital per site, next neighbor hopping matrix elements $t_{ij} = -t$) on a 2 dimensional square lattice:

$$H = -t \sum c_i^\dagger c_j + U \sum n_{i\uparrow} n_{i\downarrow}. \quad (4)$$

The band width for this model is $W = 8t$.

We first introduce the Gutzwiller Ansatz as a suitable trial function Ψ_T for the above Hamiltonian. Expectation values for the Gutzwiller function can be calculated using variational Monte Carlo (VMC). Then we describe the fixed-node diffusion Monte Carlo (FN-DMC) method that allows us to calculate more accurate variational estimates of the ground state energy (see the lecture notes by G. Bachelet for a more complete discussion of FN-DMC). The main emphasis of our discussion will be on the optimization of the trial function both in variational and fixed-node diffusion Monte Carlo.

3.1. VARIATIONAL MONTE CARLO

A good trial function for the Hubbard model has to balance the opposing tendencies of the hopping term and the interaction term: Without interaction (i.e. for $U = 0$) the ground state of the Hamiltonian (4) is the Slater determinant Φ that maximizes the kinetic energy. Without hopping ($t = 0$) the interaction is minimized. Since only doubly occupied sites, i.e. sites with $n_{i\uparrow} = 1$ and $n_{i\downarrow} = 1$, contribute to the Coulomb energy, the electrons are distributed as uniformly as possible over the lattice to minimize the number of double occupancies. A good compromise between these two extremes is to start from the non-interacting wavefunction Φ but reduce the weight of configurations R with large double occupancies $D(R)$. This leads (up to normalization) to the Gutzwiller wavefunction [9]:

$$\Psi_T(R) = g^{D(R)} \Phi(R), \quad (5)$$

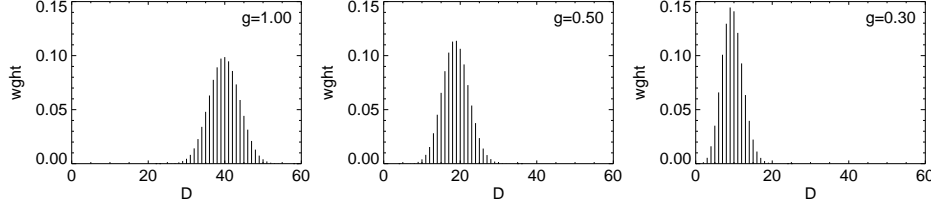


Figure 3. Weight of configurations with given number D of double occupancies for Gutzwiller wavefunctions $\Psi_T(R) = g^{D(R)} \Phi(R)$. Reducing the Gutzwiller factor g suppresses configurations with high Coulomb energy $E_{\text{Coul}}(R) = U D(R)$ at the expense of increasing the kinetic energy. The results shown here are for a Hubbard model with 16×16 sites and $101 + 101$ electrons.

with $g \in (0, 1]$ the Gutzwiller parameter. Figure 3 shows how decreasing the Gutzwiller factor suppresses the configurations with a large number of double occupancies.

To calculate the energy expectation value for the Gutzwiller wavefunction we have to perform a sum over all configurations R :

$$E_T = \frac{\langle \Psi_T | H | \Psi_T \rangle}{\langle \Psi_T | \Psi_T \rangle} = \frac{\sum_R E_{\text{loc}}(R) \Psi_T^2(R)}{\sum_R \Psi_T^2(R)}, \quad (6)$$

where we have introduced the local energy for a configuration R

$$E_{\text{loc}}(R) = \sum_{R'} \frac{\langle \Psi_T | R' \rangle \langle R' | H | R \rangle}{\langle \Psi_T | R \rangle} = \sum_{R'} t \frac{\Psi_T(R')}{\Psi_T(R)} + U D(R). \quad (7)$$

Since the number of configurations R grows exponentially with system-size, the summation in (6) can be performed only for very small systems. For larger problems we use variational Monte Carlo [10]. The idea is to perform a random walk in the space of configurations, with transition probabilities $p(R \rightarrow R')$ chosen such that the configurations R_{VMC} in the random walk have the probability distribution function $\Psi_T^2(R)$. Then

$$E_{\text{VMC}} = \frac{\sum_{R_{\text{VMC}}} E_{\text{loc}}(R_{\text{VMC}})}{\sum_{R_{\text{VMC}}} 1} \approx \frac{\sum_R E_{\text{loc}}(R) \Psi_T^2(R)}{\sum_R \Psi_T^2(R)} = E_T. \quad (8)$$

The transition probabilities can be determined from detailed balance

$$\Psi_T^2(R) p(R \rightarrow R') = \Psi_T^2(R') p(R' \rightarrow R) \quad (9)$$

which gives $p(R \rightarrow R') = 1/N \min[1, \Psi_T^2(R')/\Psi_T^2(R)]$, with N being the maximum number of possible transitions. It is sufficient to consider only

transitions between configurations that are connected by the Hamiltonian, i.e. transitions in which one electron hops to a neighboring site. The standard prescription is then to propose a transition $R \rightarrow R'$ with probability $1/N$ and accept it with probability $\min[1, \Psi_T^2(R')/\Psi_T^2(R)]$. This works well for U not too large. For strongly correlated systems, however, the random walk will stay for long times in configurations with a small number of double occupancies $D(R)$, since most of the proposed moves will increase D and hence be rejected with probability $\approx 1 - g^{D(R')-D(R)}$.

Fortunately there is a way to integrate-out the time the walk stays in a given configuration. To see how, we first observe that for the local energy (7) the ratio of the wavefunctions for all transitions induced by the Hamiltonian have to be calculated. This in turn means that we also know all transition probabilities $p(R \rightarrow R')$. We can therefore eliminate any rejection (i. e. accept with probability one) by proposing moves with probabilities

$$\tilde{p}(R \rightarrow R') = \frac{p(R \rightarrow R')}{\sum_{R'} p(R \rightarrow R')} = \frac{p(R \rightarrow R')}{1 - p_{\text{stay}}(R)}. \quad (10)$$

Checking detailed balance (9) we find that now we are sampling configurations \tilde{R}_{VMC} from the probability distribution function $\Psi_T^2(R) (1 - p_{\text{stay}}(R))$. To compensate for this we assign a weight $w(R) = 1/(1 - p_{\text{stay}}(R))$ to each configuration R . The energy expectation value is then given by

$$E_T \approx \frac{\sum_{\tilde{R}_{VMC}} w(\tilde{R}_{VMC}) E_{\text{loc}}(\tilde{R}_{VMC})}{\sum_{\tilde{R}_{VMC}} w(\tilde{R}_{VMC})}. \quad (11)$$

The above method is quite efficient since it ensures that in every Monte Carlo step a new configuration is created. Instead of staying in a configuration where Ψ_T is large, this configuration is weighted with the expectation value of the number of steps the simple Metropolis algorithm would stay there. This is particularly convenient for simulations of systems with strong correlations: Instead of having to do longer and longer runs as U is increased, the above method produces, for a fixed number of Monte Carlo steps, results with comparable error estimates.

Correlated sampling

We now turn to the problem of optimizing the trial function Ψ_T . A criterion for a good trial function is e.g. a low variational energy. To find the wavefunction that minimizes the variational energy we could do independent VMC calculations for a set of different trial functions. It is, however, difficult to compare the energies from these calculations since each VMC result comes with its own statistical errors. This problem can be avoided with correlated sampling [11]. The idea is to use the same random walk for

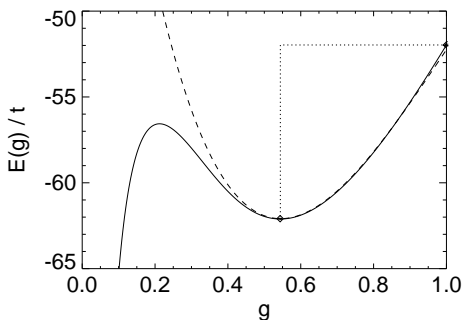


Figure 4. Correlated sampling for the Gutzwiller parameter g . The calculations are for a Hubbard model with 8×8 sites, $28 + 28$ electrons, and $U = 4t$. The full curve shows the result starting from a calculation with $g = 1$. The predicted minimum g_{\min} is indicated by the dotted line. A dashed line gives the correlated sampling curve obtained from a calculation using g_{\min} in the trial function. Both find the same minimum. $E(g)$ becomes unreliable for very small g due to reweighting factors much larger than unity.

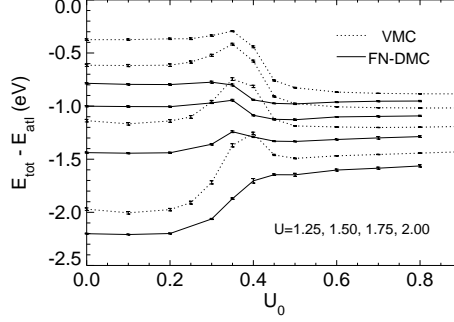
calculating the expectation value of all the different trial functions. This reduces the *relative* errors and hence makes it easier to find the minimum.

Let us assume we have generated a random walk R_{VMC} using Ψ_T as a trial function. Using the same random walk, we can then estimate the energy expectation value (8) for a different trial function $\tilde{\Psi}_T$, by introducing the reweighting factors $\tilde{\Psi}_T^2(R)/\Psi_T^2(R)$:

$$\tilde{E}_T \approx \frac{\sum_{R_{VMC}} \tilde{E}_{\text{loc}}(R) \tilde{\Psi}_T^2(R)/\Psi_T^2(R)}{\sum_{R_{VMC}} \tilde{\Psi}_T^2(R)/\Psi_T^2(R)}. \quad (12)$$

(Since the random walk R_{VMC} has only a finite number of configurations, this will only work well as long as the reweighting factors do not deviate too much from unity. Otherwise a few configurations with large reweighting factors will dominate. See Fig. 4.) We notice that (also in \tilde{E}_{loc}) the new trial function $\tilde{\Psi}_T$ appears only in ratios with the old trial function. For Gutzwiller functions (5) that differ only in the Gutzwiller factor this means that the Slater determinants cancel, leaving only powers $(\tilde{g}/g)^{D(R)}$. Since $D(R)$ is *integer* we can then rearrange the sums in (12) into polynomials in \tilde{g}/g . To find the optimal Gutzwiller parameter we then pick a reasonable g , perform a VMC run for $\Psi_T(g)$ during which we also estimate the coefficients for these polynomials. We can then calculate $E(\tilde{g})$ by simply evaluating the ratio of the polynomials. Since there are typically only of the order of some ten non-vanishing coefficients (cf. the distribution of weights in Fig. 3), this method is very efficient. Figure 4 shows how the method performs in practice. The idea of rewriting the sum over configurations into a polynomial can be easily generalized to trial functions with more correlation factors of the type $r^{c(R)}$, as long as the correlation function $c(R)$ is integer-valued on the space of configurations.

Figure 5. Dependence of variational (VMC) and fixed-node diffusion Monte Carlo (FN-DMC) on the trial function. U_0 is the Hubbard interaction that was used for the Slater determinant in the Gutzwiller wavefunction $\Psi_T(R) = g^{D(R)} \Phi(U_0)$. The Gutzwiller parameter has always been optimized. The results shown here are the energies (relative to the atomic limit) for a Hamiltonian that describes K_3C_{60} (32 sites), with U being varied from 1.25 (lowest curve) to 2.00 eV (highest curve).



Character of the Slater determinant

So far we have always constructed the Gutzwiller wavefunction from the ground state Φ of the non-interacting Hamiltonian ($U = 0$). Alternatively we could use the Slater determinant $\Phi(U)$ from solving the interacting problem in the Hartree-Fock approximation. We can even interpolate between these two extremes by doing a Hartree-Fock calculation with a fictitious Hubbard interaction U_0 to obtain the Slater determinant $\Phi(U_0)$. This introduces an additional variational parameter in the Gutzwiller wavefunction. Increasing U_0 will change the character of the trial function from paramagnetic to antiferromagnetic. This transition is also reflected in the variational energies, as is shown in Figure 5. Clearly, for small U the paramagnetic state is favorable, while for large U the antiferromagnetic state gives a lower variational energy. We notice that for all values of U the optimal U_0 is much smaller than U .

3.2. FIXED-NODE DIFFUSION MONTE CARLO

Diffusion Monte Carlo [12] allows us, in principle, to sample the true ground state of a Hamiltonian. The basic idea is to use a projection operator that has the lowest eigenstate as a fixed point. For a lattice problem where the spectrum is bounded $E_n \in [E_0, E_{\max}]$, the projection is given by

$$|\Psi^{(n+1)}\rangle = [1 - \tau(H - E_0)] |\Psi^{(n)}\rangle; \quad |\Psi^{(0)}\rangle = |\Psi_T\rangle. \quad (13)$$

If $\tau < 2/(E_{\max} - E_0)$ and $|\Psi_T\rangle$ has a non-vanishing overlap with the ground state, the above iteration converges to $|\Psi_0\rangle$. There is no time-step error involved. Because of the prohibitively large dimension of the many-body Hilbert space, the matrix-vector product in (13) cannot be done exactly. Instead, we rewrite the equation in configuration space

$$\sum_{R'} |R'\rangle \langle R' | \Psi^{(n+1)} \rangle = \sum_{R, R'} |R'\rangle \underbrace{\langle R' | 1 - \tau(H - E_0) | R \rangle}_{=: F(R', R)} \langle R | \Psi^{(n)} \rangle \quad (14)$$

and perform the propagation in a stochastic sense: $\Psi^{(n)}$ is represented by an ensemble of configurations R with weights $w(R)$. The transition matrix element $F(R', R)$ is rewritten as a transition probability $p(R \rightarrow R')$ times a normalization factor $m(R', R)$. The iteration (14) is then stochastically performed as follows: For each R we pick a new configuration R' with probability $p(R \rightarrow R')$ and multiply its weight by $m(R', R)$. Then the new ensemble of configurations R' with their respective weights represents $\Psi^{(n+1)}$. Importance sampling decisively improves the efficiency of this process by replacing $F(R', R)$ with $G(R', R) = \langle \Psi_T | R' \rangle F(R', R) / \langle R | \Psi_T \rangle$, so that transitions from configurations where the trial function is small to configurations with large trial function are enhanced:

$$\sum |R'\rangle \langle \Psi_T | R' \rangle \langle R' | \Psi^{(n+1)} \rangle = \sum_{R, R'} |R'\rangle G(R', R) \langle \Psi_T | R \rangle \langle R | \Psi^{(n)} \rangle. \quad (15)$$

Now the ensemble of configurations represents the product $\Psi_T \Psi^{(n)}$. After a large number n of iterations the ground state energy is then given by the mixed estimator

$$E_0 = \frac{\langle \Psi_T | H | \Psi^{(n)} \rangle}{\langle \Psi_T | \Psi^{(n)} \rangle} \approx \frac{\sum_R E_{\text{loc}}(R) w(R)}{\sum_R w(R)}. \quad (16)$$

As long as the evolution operator has only non-negative matrix elements $G(R', R)$, all weights $w(R)$ will be positive. If, however, G has negative matrix elements there will be both configurations with positive and negative weight. Their contributions to the estimator (16) tend to cancel so that eventually the statistical error dominates, rendering the simulation useless. This is the infamous sign problem. A straightforward way to get rid of the sign problem is to remove the offending matrix elements from the Hamiltonian, thus defining a new Hamiltonian H_{eff} by

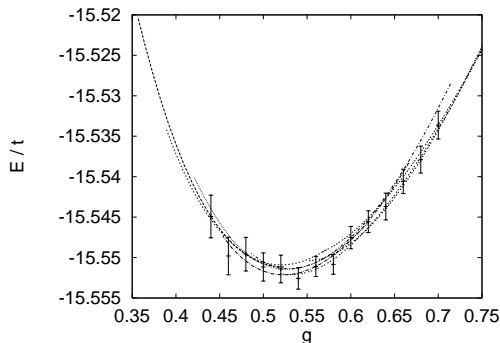
$$\langle R' | H_{\text{eff}} | R \rangle = \begin{cases} 0 & \text{if } G(R', R) < 0 \\ \langle R' | H | R \rangle & \text{else} \end{cases} \quad (17)$$

For each off-diagonal element $\langle R' | H | R \rangle$ that has been removed, a term is added to the diagonal:

$$\langle R | H_{\text{eff}} | R \rangle = \langle R | H | R \rangle + \sum_{R'} \Psi_T(R') \langle R' | H | R \rangle / \Psi_T(R). \quad (18)$$

This is the fixed-node approximation for lattice Hamiltonians introduced in Ref. [13]. H_{eff} is by construction free of the sign problem and variational, i.e. $E_0^{\text{eff}} \geq E_0$. The equality holds if $\Psi_T(R')/\Psi_T(R) = \Psi_0(R')/\Psi_0(R)$ for all R, R' with $G(R', R) < 0$.

Figure 6. Correlated sampling of the Gutzwiller parameter g in the trial function to optimize the effective Hamiltonian in fixed-node diffusion Monte Carlo. The results shown are for a Hubbard model with 4×4 sites, $7 + 7$ electrons, and $U = 4t$. The error bars are the FN-DMC energies for different values of g , the lines through the error bars are the corresponding correlated sampling curves.



Fixed-node diffusion Monte Carlo for a lattice Hamiltonian thus means that we choose a trial function from which we construct an effective Hamiltonian and determine its ground state by diffusion Monte Carlo. Because of the variational property, we want to pick the Ψ_T such that E_0^{eff} is minimized, i.e. we want to optimize the trial function, or, equivalently, the effective Hamiltonian. Also here we can use the concept of correlated sampling. For optimizing the Gutzwiller parameter g we can even exploit the idea of rewriting the correlated sampling sums into polynomials in \tilde{g}/g , that we already have introduced in VMC. There is, however, a problem arising from the fact that the weight of a given configuration $R^{(n)}$ in iteration n is given by the product $w(R^{(n)}) = \prod_{i=1}^n m(R^{(i)}, R^{(i-1)})$. Each individual normalization factor $m(R', R)$ can be written as a finite polynomial, but the order of the polynomial for $w(R^{(n)})$ increases steadily with the number of iterations. It is therefore not practical to try to calculate the ever increasing number of coefficients for the correlated sampling function $E^{(n)}(\tilde{g})$. But since we still can easily calculate the coefficients for the $m(R', R)$, we may use them to evaluate $E^{(n)}(\tilde{g})$ in each iteration on a set of predefined values \tilde{g}_i of the Gutzwiller parameter. Figure 6 shows an example. It is interesting to note that the Gutzwiller factor that minimizes E_{VMC} is usually not the optimum Gutzwiller factor for fixed-node DMC.

As in VMC we can also vary the trial function by changing the character of the Slater determinant $\Phi(U_0)$. We again find that the change from a paramagnetic to an antiferromagnetic trial function is reflected in the fixed-node energies (see Fig. 5), the paramagnetic state being favored for small U , while the antiferromagnetic state gives the lower energy for large U .

We want to use Monte Carlo methods to detect a Mott transition in the doped Fullerenes. For this we anticipate that we need an accuracy of better than 0.025 eV . To get a feeling for the accuracy of variational and fixed-node diffusion Monte Carlo, using Gutzwiller trial functions, we compare the results of the QMC calculations with exact results. Since exact diago-

Table 1. Total energy (in eV) for a cluster of four C_{60} molecules with $6 + 6$ electrons in the t_{1u} band (hopping parameters for K_3C_{60}). The results of variational and diffusion Monte Carlo are compared to the exact energy.

U	E_{exact}	E_{FN-DMC}	ΔE	E_{VMC}	ΔE
0.25	0.8457	0.8458(1)	0.000	0.8490(2)	0.003
0.50	4.1999	4.2004(1)	0.001	4.2075(3)	0.008
0.75	7.4746	7.4756(2)	0.001	7.4873(4)	0.013
1.00	10.6994	10.7004(2)	0.001	10.7179(5)	0.019
1.25	13.8860	13.8875(3)	0.002	13.9127(6)	0.027
1.50	17.0408	17.0427(4)	0.002	17.0728(7)	0.032
1.75	20.1684	20.1711(5)	0.003	20.2061(4)	0.038
2.00	23.2732	23.2757(10)	0.003	23.3125(6)	0.039

nalizations can only be done for small systems we consider a small cluster of 4 molecules. The results for different values of the Hubbard interaction U are shown in Table 1. We find that the FN-DMC error is about an order of magnitude smaller than the error in VMC. The typical FN-DMC error for our lattice model is typically some meV , which should be sufficient for the application at hand.

4. Mott transition in doped Fullerides

We now apply the quantum Monte Carlo methods described above to the Hamiltonian (3). Our aim is to understand the Mott transition in the integer-doped Fullerides A_nC_{60} . Here A stands for an alkali metal like K, Rb, or Cs. The criterion for the metal-insulator transition is the opening of the gap

$$E_g = E(N + 1) - 2E(N) + E(N - 1). \quad (19)$$

Density functional calculations predict that the doped Fullerides A_nC_{60} with $n = 1 \dots 5$ are metals [1]. Only A_6C_{60} is an insulator with a completely filled t_{1u} band. On the other hand, the strong Coulomb repulsion between two electrons on the same C_{60} molecule, which is much larger than the width of the t_{1u} band, suggests that all integer-doped Fullerides should be Mott insulators. It has therefore been suggested that experimental samples of, say, the superconductor K_3C_{60} are metallic only because they are non-stoichiometric, i.e. that they actually are $K_{3-\delta}C_{60}$ [8].

K_3C_{60}

In a first step we investigate what consequences the degeneracy of the t_{1u} -band has for the Mott transition in K_3C_{60} . The analysis is motivated by the following simple argument [14, 15]. In the limit of very large U we can estimate the energies needed to calculate the gap (19). For half filling, all molecules will have 3 electrons in the t_{1u} orbital (Fig. 7, top).

Hopping is strongly suppressed since it would increase the energy by U . Therefore, to leading order in t^2/U , there will be no kinetic contribution to the total energy $E(N)$. In contrast, the systems with $N \pm 1$ electrons have an extra electron/hole that can hop without additional cost in Coulomb energy. To estimate the kinetic energy we calculate the matrix element for the hopping of the extra charge against an antiferromagnetic background. Denoting the initial state with extra charge on molecule i by $|1\rangle$, we find that the second moment $\langle 1|H^2|1\rangle$ is given by the number of different possibilities for a next-neighbor hop times the single electron hopping matrix element t squared. By inserting $\sum_j |j\rangle\langle j|$, where $|j\rangle$ denotes the state with the extra charge hopped from site i to site j , we find $\langle 1|H|j\rangle = \sqrt{3}t$, since, with an antiferromagnetic background and degeneracy 3, there are 3 different ways an extra charge can hop to a neighboring molecule (Fig. 7, bottom). Thus, due to the 3-fold degeneracy, *the hopping matrix element is enhanced by a factor $\sqrt{3}$ compared to the single electron hopping matrix element t* . For a single electron system the kinetic energy is of the order of half the band width $W/2$. The enhancement of the hopping matrix element in the many-body case suggests then that the kinetic energy for the extra charge is correspondingly enhanced. Inserting the energies into (19) we find that for the 3-fold degenerate system our simple argument predicts a gap

$$E_g = U - \sqrt{3}W, \quad (20)$$

instead of $E_g = U - W$ in the non-degenerate case. Extrapolating to intermediate U , it appears that the degeneracy shifts the Mott transition towards larger U .

The above argument is, of course, not rigorous. First, it is not clear whether the result for E_g that was obtained in the limit of large U can be extrapolated to intermediate U , where the Mott transition actually takes place. Also the analogy of the hopping in the many-body case with the hopping of a single electron is not rigorous, since the hopping of an extra charge against an antiferromagnetic background creates a string of flipped spins [16]. Nevertheless the argument suggests that orbital degeneracy might play an important role for the Mott transition.

To test this proposition, we have performed quantum Monte Carlo calculations for the model Hamiltonian (3) with hopping matrix elements appropriate for K_3C_{60} [14]. The Coulomb interaction U has been varied from $U = 0 \dots 1.75 \text{ eV}$ to study the opening of the gap. Since the Monte Carlo calculations are for finite systems, we have to extrapolate to infinite system size. To improve the extrapolation we correct for finite-size effects:

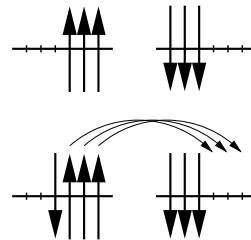


Figure 7. : Degeneracy argument.

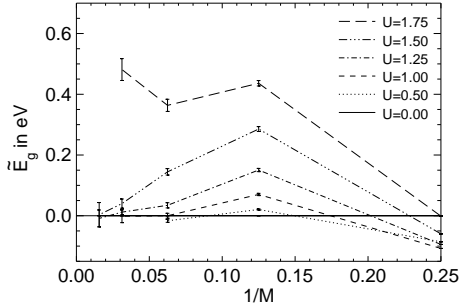


Figure 8. Finite-size corrected gap $\tilde{E}_g = E_g - U/M - E_g(U = 0)$ for increasing Coulomb interaction U as a function of $1/M$, where M is the number of molecules. The calculations are for a Hubbard model with hopping matrix elements appropriate for K_3C_{60} . The band width varies between $W = 0.58 \text{ eV}$ for $M = 4$ and $W = 0.63 \text{ eV}$ in the infinite-size limit.

First, there could be a gap $E_g(U = 0)$ already in the spectrum of the non-interacting system. Further, even for a metallic system of M molecules there will be a finite-size contribution of U/M to the gap. It comes from the electrostatic energy of the extra charge, uniformly distributed over all sites. Both corrections vanish in the limit $M \rightarrow \infty$, as they should. The finite-size corrected gap $\tilde{E}_g = E_g - U/M - E_g(U = 0)$ for systems with $M = 4, 8, 16, 32$, and 64 molecules is shown in Figure 8. We find that the gap opens for U between 1.50 eV and 1.75 eV . Since for the real system $U = 1.2 \dots 1.4 \text{ eV}$, K_3C_{60} is thus close to a Mott transition, but still on the metallic side – even though U is considerably larger than the band width W . This is in contrast to simpler theories that neglect orbital degeneracy.

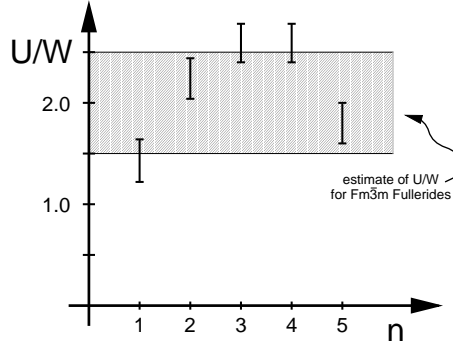
Doping dependence

The degeneracy argument described above for K_3C_{60} can be generalized to integer fillings. Away from half filling the enhancement of the hopping matrix elements for an extra electron is different from that for an extra hole. The effective enhancement for different fillings are given in the adjacent table.

filling	enhancement
$n = 3$	$\sqrt{3} \approx 1.73$
$n = 2, 4$	$\frac{\sqrt{3}+\sqrt{2}}{2} \approx 1.57$
$n = 1, 5$	$\frac{\sqrt{2}+1}{2} \approx 1.21$

We find that the enhancement decreases as we move away from half filling. Therefore we expect that away from half filling, correlations become more important, putting the system closer to the Mott transition, or maybe even pushing it across the transition, making it an insulator. We have analyzed the doping dependence of the Mott transition for the same Hamiltonian as used for K_3C_{60} , changing the filling of the t_{1u} band from $n = 1$ to 5 [17]. This model describes the $\text{Fm}\bar{3}\text{m}$ -Fullerides A_nC_{60} with fcc lattice and orientational disorder [18]. The critical Coulomb interaction U_c , at which the transition from a metal (for $U < U_c$) to an insulator ($U > U_c$) takes place, is shown in Figure 9 for the different integer fillings. As ex-

Figure 9. Doping dependence of the Mott transition. The error bars indicate the estimate of the critical ratio U_c/W for different integer fillings of the t_{1u} band. The calculations are for doped Fm $\bar{3}m$ Fullerenes with fcc lattice structure and orientational disorder. The shaded region shows the range of U/W in which the doped Fullerenes are falling.



pected from the degeneracy argument, U_c decreases away from $n = 3$. We note, however, that U_c is asymmetric around half filling. This asymmetry is not present in the simple degeneracy argument, where we implicitly assumed that the lattice is bipartite. In such a situation we have electron-hole symmetry, which implies symmetry around half-filling. For frustrated lattices like the fcc lattice electron-hole symmetry is broken, leading to the asymmetry in U_c that is seen in Fig. 9.

Lattice dependence

To understand the effect of frustration in terms of the hopping arguments that we have made so far, we have to consider more than just one next-neighbor hop. The simplest system where we encounter frustration is a triangle with hopping between neighboring sites. In the single electron case we can form a bonding state with energy $E_{\min} = 2t$, but because of frustration we cannot form an antibonding state. Instead the maximum eigenenergy is $E_{\max} = t$. Hence frustration leads to an asymmetric 'band' of width $W = 3t$.

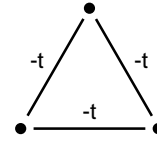


Figure 10. : Triangle

In the many-body case the situation is different. Like in the degeneracy argument we look at the hopping of an extra electron against a (frustrated) antiferromagnetic background in the large- U limit. For simplicity we assume a non-degenerate system, i.e. there is one electron per site on the triangle, plus the extra electron. In this case we have to move the extra charge *twice* around the triangle to come back to the many-body state we started from. Thus in the large- U limit the many-body problem is an eigenvalue problem of a 6×6 matrix with extreme eigenvalues $\pm 2t$. In the degeneracy argument we have assumed that the kinetic energy of the extra charge is given by $W/2$. On the triangle, we find, however, that the hopping energy is larger than that by a factor $4/3$. This suggests that for frustrated systems the single electron band width W in (20) should be multiplied by a prefactor

larger than one. We therefore expect that frustration alone, even without degeneracy, shifts the Mott transition to larger U .

To analyze the effect of frustration on the Mott transition we have determined the critical U for a hypothetical doped Fulleride A_4C_{60} with body centered tetragonal (bct) structure, a lattice without frustration, having the same band width ($W = 0.6 \text{ eV}$) as the fcc-Fullerides, shown in Figure 9. For $U = 1.3 \text{ eV}$, we find a gap $E_g \approx 0.6 \text{ eV}$ for the Fulleride with bct structure, while the frustrated fcc compound is still metallic $E_g = 0$. This difference is entirely due to the lattice structure. Using realistic parameters for K_4C_{60} [5] that crystallizes in a bct structure we find a Mott insulator with gap $E_g \approx 0.7 \text{ eV}$, which is in line with experimental findings: $E_g = 0.5 \pm 0.1 \text{ eV}$ [19].

Conclusion

We have seen that, due to more efficient hopping, orbital degeneracy increases the critical U at which the Mott transition takes place. This puts the integer-doped Fullerides close to a Mott transition. Whether they are on the metallic or insulating side depends on the filling of the band and the lattice structure: Since the degeneracy enhancement works best for a half filled band, systems doped away from half-filling tend to be more insulating. The effect of frustration, on the other hand, is to make the system more metallic.

Acknowledgments

This work has been supported by the Alexander-von-Humboldt Stiftung under the Feodor-Lynen-Program and the Max-Planck-Forschungspreis.

References

1. Erwin, S. C. (1993) Electronic Structure of the Alkali-Intercalated Fullerides, Endohedral Fullerenes, and Metal-Adsorbed Fullerenes, in W. E. Billups and M. A. Ciufolini (Eds.), *Buckminsterfullerenes*, VCH Publishers, New York, pp. 217-253
2. Löwdin, P. O. (1951) A Note on the Quantum-Mechanical Perturbation Theory, *J. Chem. Phys.* **19**, 1396
3. see e.g. Inversion by Partitioning, in W. H. Press, B. P. Flannery, S. A. Teukolsky, and W. T. Vetterling, *Numerical Recipes in Fortran: The Art of Scientific Computing*, Cambridge University Press, 1992, p. 70
4. Gunnarsson, O., Satpathy, S., Jepsen, O., and Andersen, O. K. (1991) Orientation of C_{60} Clusters in Solids, *Phys. Rev. Lett.* **67**, 3002 Satpathy, S., Antropov, V. P., Andersen, O. K., Jepsen, O., Gunnarsson, O., and Liechtenstein, A. I. (1992) Conduction-band structure of alkali-metal-doped C_{60} , *Phys. Rev. B* **46**, 1773;
5. Gunnarsson, O., Erwin, S. C., Koch, E., and Martin, R. M. (1998) Role of alkali atoms in A_4C_{60} , *Phys. Rev. B* **57**, 2159
6. Antropov, V. P., Gunnarsson, O., and Jepsen, O. (1992) Coulomb integrals and model Hamiltonians for C_{60} , *Phys. Rev. B* **46**, 13647

7. Brühwiler, P. A., Maxwell, A. J., Nilsson, A., Mårtensson, N., and Gunnarsson, O. (1993) Auger and photoelectron study of the Hubbard U in C_{60} , K_3C_{60} , and K_6C_{60} , *Phys. Rev. B* **48**, 18296
8. Lof, R. W., van Veenendaal, M. A., Koopmans, B., Jonkman, H. T. and Sawatzky, G. A. (1992) Band Gap, Excitons, and Coulomb interaction in solid C_{60} , *Phys. Rev. Lett.* **68**, 3924
9. Gutzwiller, M. C. (1963) Effect of correlation on the ferromagnetism of transition metals, *Phys. Rev. Lett.* **10**, 159
10. Horsch, P. and Kaplan, T. A. (1983) Exact and Monte Carlo studies of Gutzwiller's state for the localised-electron limit in one dimension, *J. Phys. C* **16**, L1203; Metropolis, N., Rosenbluth, A. W., Rosenbluth, N. M., Teller, A. H., and Teller, E. (1953) Equation of State Calculations by Fast Computing Machines, *J. Chem. Phys.* **21**, 1087
11. Ceperley, D. M., Chester, G. V., and Kalos, M. H. (1977) Monte Carlo simulation of a many-Fermion study, *Phys. Rev. B* **16**, 3081; Umrigar, C. J., Wilson, K. G., and Wilkins, J. W. (1988) Optimized Trial Wave Functions for Quantum Monte Carlo Calculations, *Phys. Rev. Lett.* **60**, 1719
12. Trivedi, N. and Ceperley, D. M. (1989) Green-function Monte Carlo study of quantum antiferromagnets, *Phys. Rev. B* **40**, 2737
13. ten Haaf, D. F. B., van Bemmelen, H. J. M., van Leeuwen, J. M. J., and van Saarloos, W. (1994) Fixed-node quantum Monte Carlo method for lattice Fermions, *Phys. Rev. Lett.* **72**, 2442; ten Haaf, D. F. B., van Bemmelen, H. J. M., van Leeuwen, J. M. J., van Saarloos, W. and Ceperley, D. M. (1995) Proof for an upper bound in fixed-node Monte Carlo for lattice Fermions, *Phys. Rev. B* **51**, 13039
14. Gunnarsson, O., Koch, E., and Martin, R. M. (1996) Mott transition in degenerate Hubbard models: Application to doped Fullerenes, *Phys. Rev. B* **54**, R11026
15. Gunnarsson, O., Koch, E., and Martin, R. M. (1997) Mott-Hubbard insulators for systems with orbital degeneracy, *Phys. Rev. B* **56**, 1146
16. We note that this does not happen for the hopping of an extra charge against a *ferromagnetic* background. For a non-degenerate, bipartite system the ferromagnetic arrangement is actually favorable (Nagaoka's theorem, Y. Nagaoka (1966) *Phys. Rev. B* **147**, 392), but for a system with orbital degeneracy N an antiferromagnetic background seems in general more favorable, since hopping can then take place in N channels.
17. Koch, E., Gunnarsson, O., and Martin, R. M. (1998) Quantum Monte Carlo calculations for integer-doped Fullerides, in H. Kutzmany, J. Fink, M. Mehring, and S. Roth (Eds.), *Molecular Nanostructures*, World Scientific Publishing Company, Singapore, pp. 235-238
18. Gunnarsson, O. (1997) Superconductivity in Fullerides, *Rev. Mod. Phys.* **69**, 575
19. Knupfer, M. and Fink, J. (1997) Mott-Hubbard-like Behavior of the Energy Gap of A_4C_{60} ($A=Na, K, Rb, Cs$) and $Na_{10}C_{60}$, *Phys. Rev. Lett.* **79**, 2714